Osaka, Japan, June 21-26, 2009

ISBN 978-1-880653-53-1 (Set); ISSN 1098-618

Underwater Thruster Saturation Detection and Prevention Considering Battery Voltage Sag

[1]Aaron M. Hanai, [2]Giacomo Marani, [1]Kaikala H. Rosa, [2]Song K. Choi

[1]Marine Autonomous Systems Engineering, Inc.
Honolulu, HI, USA

[2]University of Hawai`i at Manoa, College of Engineering
Honolulu, HI, USA

ABSTRACT

This paper reports on the development of a control module that detects and effectively prevents thruster saturation for an autonomous underwater vehicle (AUV). A model has been developed to approximate the maximum available thrust, per thruster, as a function of the battery voltage sag. A thruster would be considered to be in saturation if its reference input exceeds its particular output limit. This ratio can be expressed as a scalar value, which can be used to adjust the reference thrust vector that is fed to the thruster control system. This approach can minimize the total error vector in the vehicle kinematics.

KEY WORDS:
Thruster; saturation; model; AUV.

INTRODUCTION

The primary goal of this effort is to prevent thruster saturation as applied to an AUV. This can be accomplished by exposing some of the underlying reasons for the saturation conditions. These issues can therefore be managed at a low-level before they have the opportunity to cause problems with the high-level control system.

Ultimately, it is the function of the vehicle control system to issue reference thruster force values within the presumed known saturation limits. This can be accomplished by techniques such as dynamic state feedback (Sarkar, Podder, Antonelli, 2002) or bounded infinity-norm allocation (Soylu, Buckham, Podhorodeski, 2007) for example. However, it is still possible for unmodeled errors or hardware faults to cause saturation conditions, resulting in poor controller performance (Smallwood and Whitcomb, 2002; Smallwood and Whitcomb, 2004).

Preemptively avoiding thruster saturation limits may yet result in errors because these limits are not necessarily constant, but a function of the power source, which is commonly comprised of batteries for an AUV. If this battery supply is low on energy, then it would be unable to provide the required electric current to the thrusters, which consequently translates to a loss in maximum available thrust. It is therefore imperative to understand this relationship in order to model the variable saturation limits, and predict the eventual loss of available thrust. In this case, an algorithm has been developed to minimize the impact of these saturation errors on the vehicle trajectory. An AUV with n thrusters must have some sort of thruster control module whose function is to perform transformations between n reference thrust values and a 6 degree-of-freedom body-fixed force vector. The key to minimizing the overall trajectory error is to keep track of the particular thruster that has the maximum saturation error and scale the entire n-element thruster force vector according to values derived from that specific thruster.

Practical experiments were performed to measure the degradation of thruster output as a function of the sagging battery source voltage, as well as to determine the maximum attainable thrust for each thruster. This procedure was performed in a small indoor test tank by attaching a thruster to a lever-based test rig and measuring the force via load cell. The resulting data is a function of the input command voltage, propeller shaft velocity, motor current, and battery voltage, all of which are measurable quantities. In practice, a thruster that is not in saturation at the beginning of a mission may later become saturated when the thrust limit decreases due to the reduced battery voltage over the course of that mission.

Fig. 1 SAUVIM.

VEHICLE DESCRIPTION

The application and development aspects of the presented research work was performed on the Semi-Autonomous Underwater Vehicle for Intervention Missions (SAUVIM) (Yuh and Choi, 1999) shown during deployment in Fig. 1. It is a joint project between Marine Autonomous

Systems Engineering, Inc. (MASE, Inc.), the Autonomous Systems Laboratory of the University of Hawai`i at Manoa College of Engineering, and the Naval Undersea Warfare Center, Rhode Island. SAUVIM is capable of intervention tasks because of its electronic 7 joint robotic manipulator, which is itself autonomous, forming a 13 degree of freedom Underwater Vehicle-Manipulator System (UVMS).

Hardware Overview

The vehicle is designed for untethered, full-ocean depth autonomous operation. As such, it is outfitted with an array of sensors including a Photonic Inertial Navigation System (PHINS), Doppler Velocity Logger (DVL), two imaging sonars, six sonar altimeters, GPS, depth sensors, etc. For fine-motion control and system robustness, the vehicle is equipped with eight thrusters as arranged in Fig. 2.

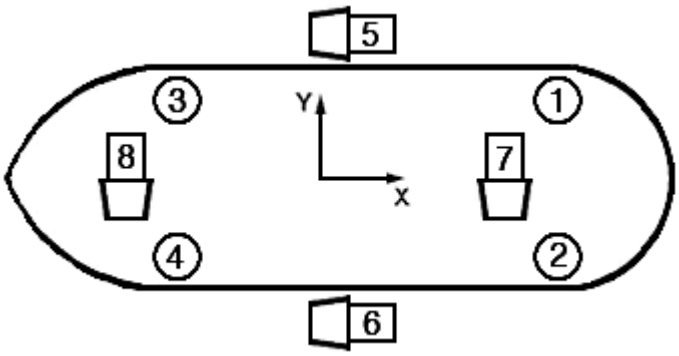

Fig. 2 Thruster layout: top view with x-axis toward the bow.

Power Subsystem

For system robustness, different operational subsystems are driven by separate battery supplies. There are three isolated lead-acid battery banks for the 24V vehicle navigation computer, 24V manipulator computer, and 72V manipulator motor controllers. The thrusters are powered by a 144V NiMH battery bank. In detail, the thruster power system is actually comprised of a bank of 48 rechargeable NiMH batteries rated at 144V 3Ah apiece. Each of these is comprised of 120 series-connected 1.2V 3Ah cells that were spot welded together and housed in pressure tubes. A junction box housed in a pressure vessel on the vehicle allows the 48 batteries to be charged and tested separately, but also to be tied together in parallel for a total battery capacity of 144V 144Ah available to the thrusters.

THRUSTER SATURATION

The approach to detect and prevent thruster saturation is put into effect by means of a two part prevention scheme. First, the modeling of the battery power system provides an approximation function for the maximum available thrust at any time, and therefore the saturation limits. It is the function of the high-level navigation control system to issue reference thrust commands that are within these limits. However, unforeseen errors may still result in thruster saturation. The second aspect of the saturation prevention algorithm is to minimize the error due to saturation by scaling back the reference thruster values within the low-level thruster control system.

Thruster Control System

Some background information must first be provided in order to describe the application of the thruster saturation prevention. The body force vector τ is the input to the underwater vehicle equation of motion (Fossen, 1994) given by

$$M(q)\dot{p} + D(q,p)p + g(q) = \tau \tag{1}$$

where p is the linear and angular velocities in the body-fixed frame and q is the vehicle position and orientation vector in the earth-fixed frame. M is the inertia matrix, including both rigid body and added mass terms. D is the matrix of dissipative terms including Coriolis and centripetal effects, as well as hydrodynamic damping. The vector g describes the gravitational and buoyant restoring forces. Given sensor feedback data $q, p, \dot{p}$, the function of the navigation controller is to generate the reference vector τ. This body force vector must be transformed to a thruster force vector $T = [T_1 \ \cdots \ T_n]$ according to the thruster layout shown in Fig. 2. From the thruster positions and orientations x_i and r_i respectively, together with the vehicle center of mass $C = [C_x, C_y, C_z]$, then

$$\tau = KT \tag{2}$$

given the transformation matrix

$$K \triangleq \begin{bmatrix} (x_1 - C)\times r_1 & \cdots & (x_n - C)\times r_n \\ r_1 & \cdots & r_n \end{bmatrix}. \tag{3}$$

The thruster force vector is then represented by inverting Eq. 2 so that

$$T = K^{\#}\tau \tag{4}$$

according to the generalized inverse (Nakamura, 1990)

$$K^{\#} \triangleq K^T \left(KK^T\right)^{-1} \tag{5}$$

that minimizes the error norm $\|\tau - KT\|$.

Saturation Guard

The algorithm and software module for thruster saturation detection and prevention is referred to by the SAUVIM group as the *Saturation Guard*. The nomenclature is fairly accurate as it is an inclusive safeguard against thruster saturation by means of a preventive component that attempts to predict the thruster limits, and an accommodation component that minimizes the errors resulting from any failure of the initial prediction step. The details of the thrust limit approximation function are primarily empirical in nature, and the experimental investigation is described in the next section. It will be demonstrated that the maximum available thrust can be approximated by the measured battery voltage. Hence for a vehicle with n thrusters, each individual thrust limit is a known quantity $(T_{lim})_i$ for thruster i. Given a reference thrust $(T_r)_i$, a non-dimensional saturation index S_i can be formed by dividing the reference by the limit. Therefore, thruster i would be saturated if its index were greater than one. Since the Saturation Guard should only be implemented if one of the thrusters is actually in a saturation condition, the index should be defined

$$S_i \triangleq \begin{cases} \dfrac{(T_r)_i}{(T_{lim})_i}, & (T_r)_i > (T_{lim})_i \\ 1\ , & (T_r)_i \le (T_{lim})_i \end{cases} \tag{6}$$

To minimize the effects of the saturation error, it is necessary to scale the entire n-dimensional thruster force reference vector T_r , as in equation 4, by the maximum of the n saturation indices:

$$S_m \triangleq max(S_i) \geq 1 \tag{7}$$

Hence, the thruster force vector scaled by the Saturation Guard is

$$T_G \triangleq \left(\tfrac{1}{S_m}\right) T_r \tag{8}$$

The effects of saturation errors are best explained through a simplified example as follows. Consider the geometry of a vehicle with four thrusters, and constrained only to surge, sway, and yaw degrees of freedom. This could correspond to a vehicle like SAUVIM that would utilize only its longitudinal and lateral thrusters, as in thrusters 5 through 8 in Fig. 2. Note that the general case for SAUVIM would consist of a 6-element body force vector (surge, sway, heave, roll, pitch, yaw) and an 8-element thruster force vector. For the simplified example, equation 2 would take the form

$$\tau_r = \begin{bmatrix} \tau_{surge} \\ \tau_{sway} \\ \tau_{yaw} \end{bmatrix} = \begin{bmatrix} K_{11} & K_{12} & K_{13} & K_{14} \\ K_{21} & K_{22} & K_{23} & K_{24} \\ K_{31} & K_{32} & K_{33} & K_{34} \end{bmatrix} \begin{bmatrix} T_1 \\ T_2 \\ T_3 \\ T_4 \end{bmatrix} = KT_r \tag{9}$$

Each thruster has an associated saturation index S_i. Hence the output body force under saturation τ_S is equal to the reference body force τ_r plus some error $\tau_{e,S}$ as follows:

$$\tau_S = KT_S = K \begin{bmatrix} \left(\frac{1}{S_1}\right) T_1 \\ \left(\frac{1}{S_2}\right) T_2 \\ \left(\frac{1}{S_3}\right) T_3 \\ \left(\frac{1}{S_4}\right) T_4 \end{bmatrix} = K \begin{bmatrix} T_1 \\ T_2 \\ T_3 \\ T_4 \end{bmatrix} + K \begin{bmatrix} \left(\frac{1}{S_1}-1\right) T_1 \\ \left(\frac{1}{S_2}-1\right) T_2 \\ \left(\frac{1}{S_3}-1\right) T_3 \\ \left(\frac{1}{S_4}-1\right) T_4 \end{bmatrix} = \tau_r + \tau_{e,S} \tag{10}$$

$$\tau_{e,S} = \begin{bmatrix} K_{11} & K_{12} & K_{13} & K_{14} \\ K_{21} & K_{22} & K_{23} & K_{24} \\ K_{31} & K_{32} & K_{33} & K_{34} \end{bmatrix} \begin{bmatrix} \left(\frac{1}{S_1}-1\right) T_1 \\ \left(\frac{1}{S_2}-1\right) T_2 \\ \left(\frac{1}{S_3}-1\right) T_3 \\ \left(\frac{1}{S_4}-1\right) T_4 \end{bmatrix} = \begin{bmatrix} \sum_{i=1}^{4} K_{1i} \left(\frac{1}{S_i}-1\right) T_i \\ \sum_{i=1}^{4} K_{2i} \left(\frac{1}{S_i}-1\right) T_i \\ \sum_{i=1}^{4} K_{3i} \left(\frac{1}{S_i}-1\right) T_i \end{bmatrix} \tag{11}$$

However, if the entire vector T_r is scaled by S_m according to the Saturation Guard, then the output τ_G with error $\tau_{e,G}$ is given by

$$\tau_G = KT_G = K\left(\tfrac{1}{S_m}\right) \begin{bmatrix} T_1 \\ T_2 \\ T_3 \\ T_4 \end{bmatrix} = KT_r + \left(\tfrac{1}{S_m}-1\right) KT_r = \tau_r + \tau_{e,G} \tag{12}$$

$$\tau_{e,G} = \left(\tfrac{1}{S_m}-1\right) \tau_r \tag{13}$$

It is key to adjust the entire thruster force vector as a whole. Using the Saturation Guard, the error from equation 13 may have a non-zero magnitude, but the resulting body force output vector is parallel to the input reference because the cross product is zero for all inputs:

$$\tau_r \times \tau_G = \tau_r \times \left(\tau_r + \tau_{e,G}\right) = \tau_r \times \tau_{e,G} = \tau_r \times \left(\tfrac{1}{S_m}-1\right) \tau_r = 0 \;\; \forall \tau_r \tag{14}$$

This is an important result because it is a sufficient condition to assure that the reference input vector τ_r and the output vector τ_G will always have the same orientation when the Saturation Guard is employed. Conversely, the result will generally not hold if the Saturation Guard is not utilized, as demonstrated by the non-zero cross product of the terms from equations 10 and 11:

$$\tau_r \times \tau_S = \tau_r \times \tau_{e,S} = \begin{bmatrix} \tau_{sway} \sum_{i=1}^{4} K_{3,i} \left(\frac{1}{S_i}-1\right) T_i - \tau_{yaw} \sum_{i=1}^{4} K_{2,i} \left(\frac{1}{S_i}-1\right) T_i \\ \tau_{yaw} \sum_{i=1}^{4} K_{1,i} \left(\frac{1}{S_i}-1\right) T_i - \tau_{surge} \sum_{i=1}^{4} K_{3,i} \left(\frac{1}{S_i}-1\right) T_i \\ \tau_{surge} \sum_{i=1}^{4} K_{2,i} \left(\frac{1}{S_i}-1\right) T_i - \tau_{sway} \sum_{i=1}^{4} K_{1,i} \left(\frac{1}{S_i}-1\right) T_i \end{bmatrix} \tag{15}$$

To further exemplify the results, Fig. 3 represents a simplified, two dimensional illustrative example. The outlined arrows represent the maximum attainable thrusts, the solid lines are the component thrust forces, and the dashed line is the resultant vector. If the desired input forces are within the limits, then the actual output will be unaffected by saturation, as shown in row 1 of Fig. 3. If a desired thrust is greater than its thruster's limit, then the actual output will clip, causing both magnitude and orientation errors in the resultant vector, shown in row 2 of Fig. 3. However, employing the Saturation Guard in this situation and scaling the entire reference vector by the appropriate index, the resultant force maintains the proper orientation with an error in magnitude only, depicted in row 3 of Fig. 3.

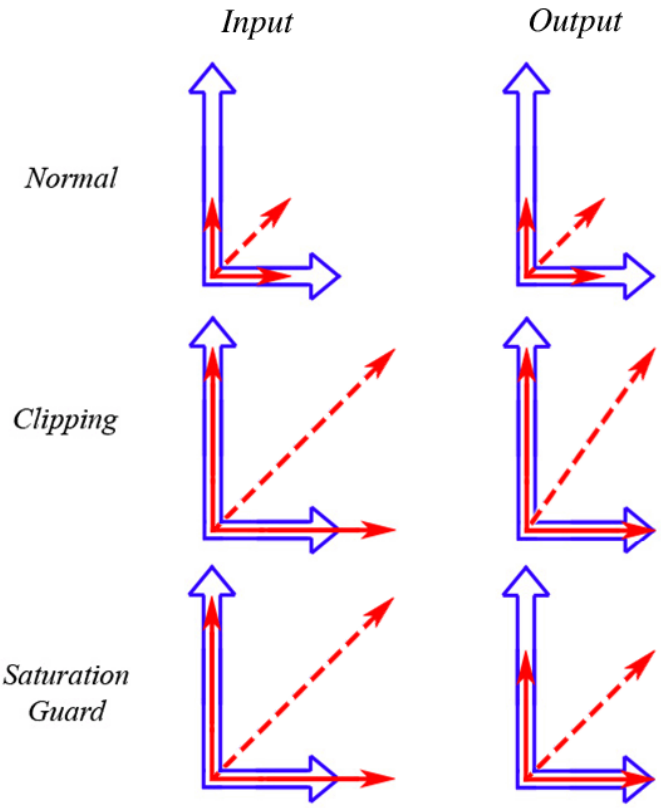

Fig. 3 Two-dimensional illustrative example.

SIMULATION AND EXPERIMENTS

This section begins by outlining the experimental procedures and results demonstrating the dependence of the maximum attainable thrust on battery voltage. This process was actually comprised of two separate experimental projects dealing with the characterization of battery properties and underwater thruster modeling, the details of which are beyond the relevance of the presented work. Following that is the continuation of the simplified vehicle model example as applied to SAUVIM. The resulting body force data are actually simulated motions that are calculated from experimentally measured thruster force responses.

Battery Discharge Experiments

A custom discharge circuit was designed and constructed in order to periodically monitor the health of the 144V NiMH battery cells. Currently, four batteries can be discharged simultaneously and the respective voltages are recorded to a computer via an A/D converter. For simplicity, each circuit discharges its battery by means of a fixed, known resistance. Time, voltage, and therefore current, can be measured and stored in order to calculate the output electric charge. The data can be compared to an analogous input charge experiment in order to determine the health of the battery. The discharge apparatus includes an automatic shut-off feature in which the voltage feedback triggers a relay that breaks the circuit when the battery voltage is below a specified level.

Fig. 4 depicts the experimental result of a resistive discharge test. All four batteries were fully charged immediately prior to this experiment. Note that battery 4 demonstrates that it was unable to hold the same amount of charge as the other three batteries. Also, the automatic shut-off failed for battery 3, which was probably detrimental to its health, but beneficially demonstrative of the characteristic profile under extreme depth of discharge.

Thruster Experiments

Experiments were performed to measure the degradation of thruster output as a function of the sagging battery source voltage. In order to collect data over long intervals at controlled voltages and currents, these specific tests were performed utilizing regulated power supplies in lieu of the batteries. The Technadyne 2010 thrusters were removed from the AUV and mounted individually on a beam-type test rig equipped with a load-cell that is connected to a computer via A/D converter. The thrusters were fully submerged in an indoor test tank of sufficient depth in order to prevent ventilation of the propeller blades. Note that ventilation occurs when air from the water surface is drawn down into the propeller blades causing slippage and therefore skewing the measured thrust data.

Fig. 5 shows a compilation of five experimental test runs measuring the output thrust as a function of input reference thrust at different power supply voltages. The thruster is unable to deliver the desired thrust as the source voltage decreases, and reaches a maximum value based on this voltage. From these experiments, the maximum attainable thrust is found to be a function of the source voltage, as indicated by the data point markers in Fig. 6. It was found that the data trends could be approximated by linear functions. The approximation functions are then stored in the thruster software control system in order to predict the maximum attainable thrust, per thruster, based on the available battery voltage.

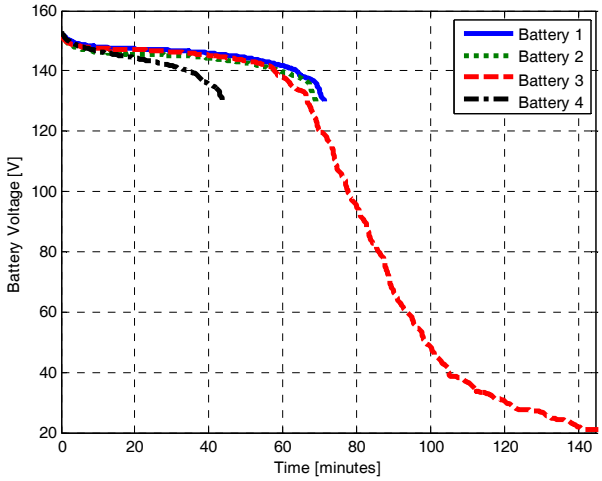

Fig. 4 Experimentally measured resistive discharge of NiMH batteries.

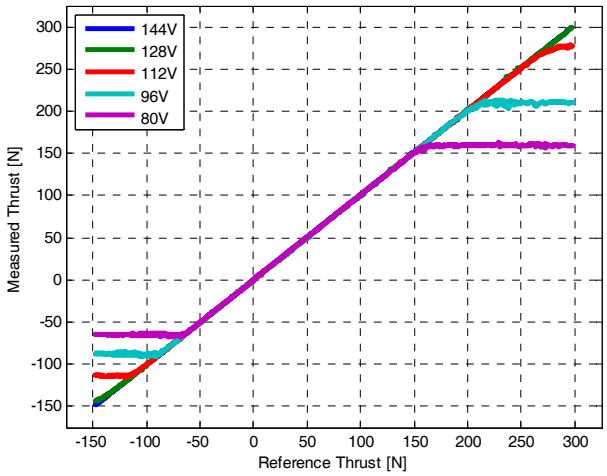

Fig. 5 Measured vs. reference thrust as a function of source voltage.

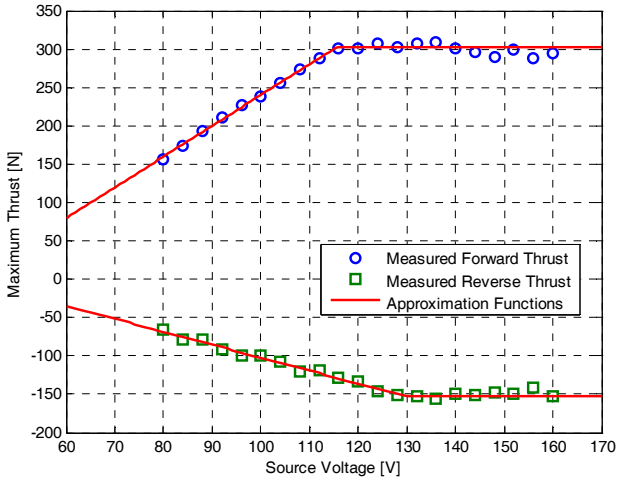

Fig. 6 Maximum available thrust vs. source voltage.

Saturation Guard Simulation and Experiments

To demonstrate the application of the Saturation Guard, the following tests utilize only two longitudinal and two lateral thrusters of SAUVIM, corresponding to thrusters 5 through 8 of Fig. 2, while constrained to planar motions of surge, sway, and yaw. The desired sample path is in the port bow direction at 45 degrees while maintaining a constant yaw angle, and then returning to the original starting pose. The trajectory of this pre-defined motion is a sinusoid with a total period of one minute and a magnitude of 400N in surge and 400N in sway, which is large enough to cause saturation of the specified thrusters. These tests utilized a regulated power supply set at 160V to maintain consistent thruster output.

The output body force results τ_S and τ_G were simulated in order to keep the focus of this work on thruster saturation. During an operational mission, the components of the thruster force vector T_r need to be accurately transformed to motor controller voltages typically by some type of model-based function (Fossen and Blanke, 2000; Bachmayer, Whitcomb, Grosenbaugh, 2000; Kim, Han, Chung, Yuh, Lee, 2005). The resulting vehicle motion would then be measured by means of various sensors to close the loop. Output body force simulation eliminates inaccuracy from the extra transformation function and compounded sensor errors.

The surge, sway, and yaw components of the reference body force vector τ_r are plotted by the markers in Fig. 7. The associated thruster force vector T_r is calculated according to equation 4 and plotted as the markers in Fig. 8. The solid lines of Fig. 8 are the resulting experimentally measured output thrusts T_S due to these inputs. Note the saturation level at about -150N which corresponds to the thrust limits measured in Fig. 6. Also note that only thrusters 7 and 8 saturate during the first 30 seconds and only thrusters 5 and 6 saturate during the last 30 seconds. These saturated thrusts are then computed via equation 2 to produce the simulated body force output τ_S represented by the solid lines in Fig. 7. The measured thruster force errors and simulated body force errors are plotted in Fig. 9 and Fig. 10 respectively.

The same desired body force τ_r and associated thruster force T_r is represented by the markers in Fig. 11 and Fig. 12 respectively. However, the measured output thruster force T_G, shown in solid lines, is scaled by the Saturation Guard according to equation 8. As before, only thrusters 7 and 8 saturate during the first 30 seconds, and only thrusters 5 and 6 in the last 30 seconds, but all four thrusters are scaled by the same relative amount in each instance. This yields the simulated body force τ_G as the solid lines in Fig. 11. The corresponding thruster force and body force errors are plotted in Fig. 13 and Fig. 14 respectively. The key result is that the body force error subject to the Saturation Guard $\tau_{e,G}$ is a scalar multiple of the reference input τ_r as was predicted by equation 13, and the resulting output trajectory therefore maintains the proper orientation as predicted by equation 14.

CONCLUSIONS

An empirically verified model has been developed to approximate the maximum attainable thrust from a thruster, based on the available source voltage. An algorithm has also been developed to minimize the effect of unmodeled thruster saturation. This has been mathematically proven to limit the error to magnitude alone, preserving the reference orientation. It has also been verified by experiment in the thruster force domain, and by simulation in the final transformation step to the body force domain.

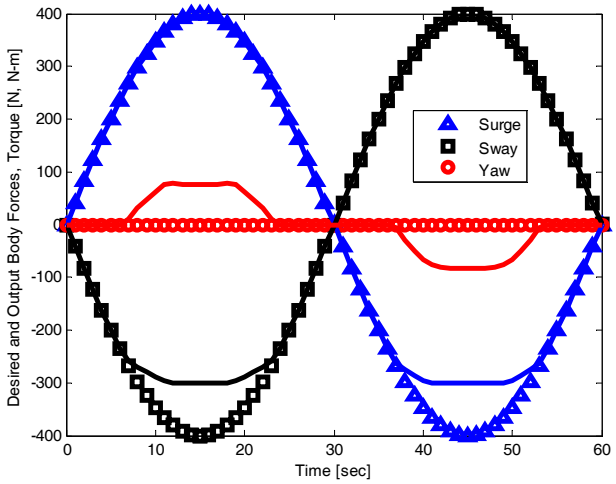

Fig. 7 Markers denote the desired body force. Solid lines denote the simulated output body force as a result of saturation.

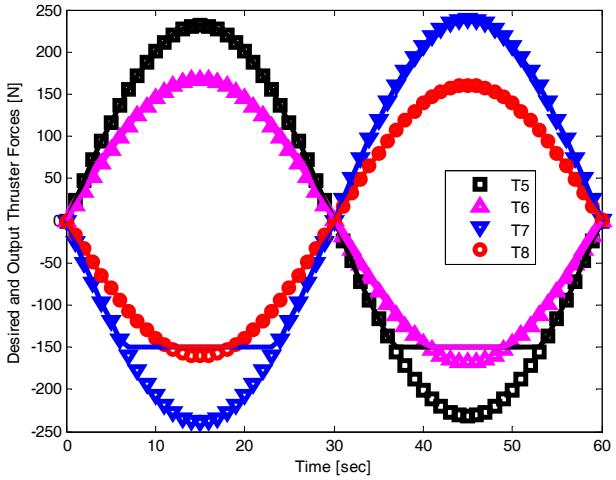

Fig. 8 Markers denote the desired thruster force. Solid lines denote the measured output thruster force as a result of saturation.

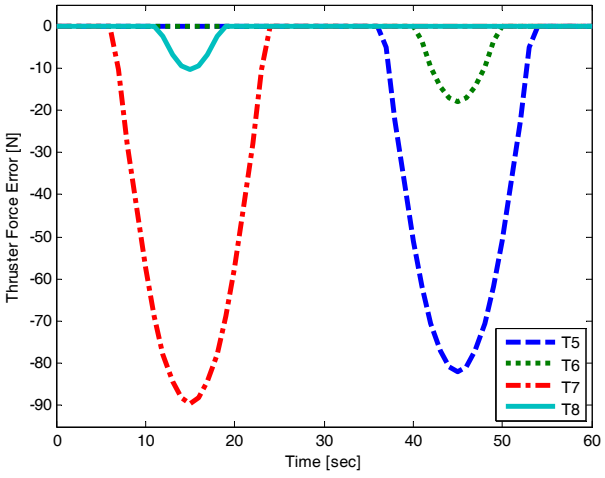

Fig. 9 Measured thruster force error as a result of saturation.

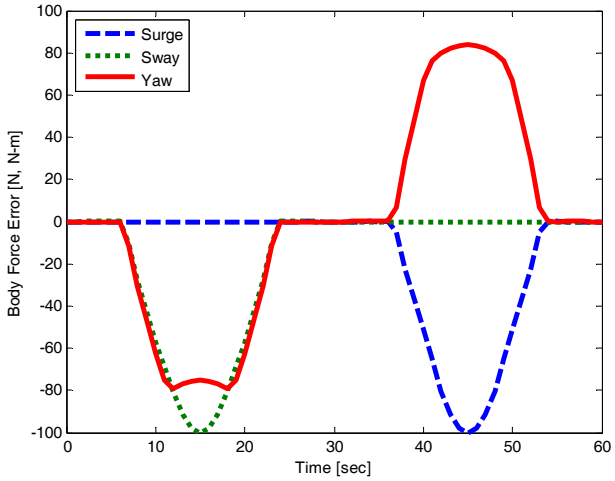

Fig. 10 Simulated body force error as a result of saturation.

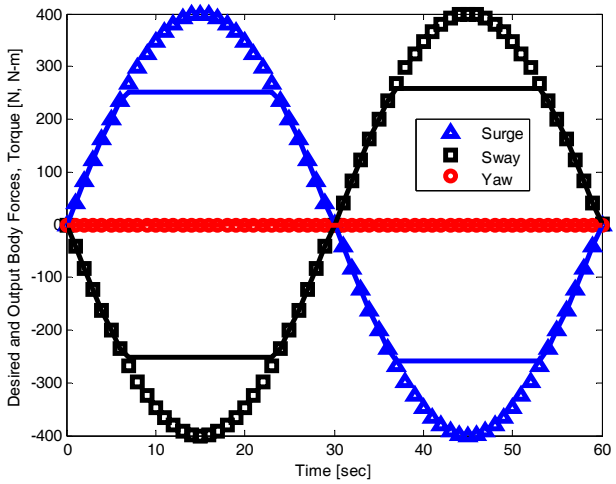

Fig. 11 Markers denote the desired body force. Solid lines denote the simulated output body force using Saturation Guard.

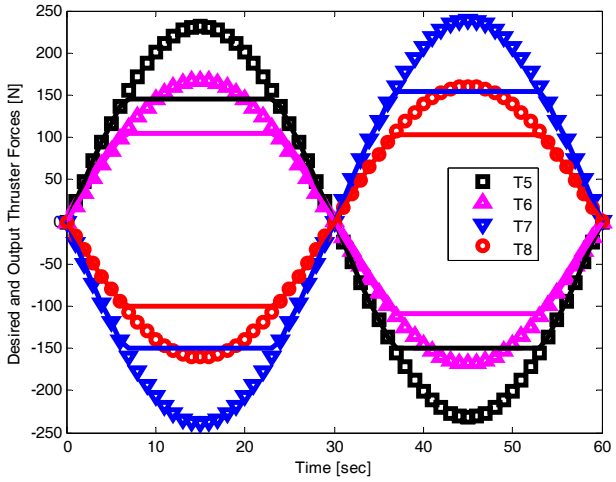

Fig. 12 Markers denote the desired thruster force. Solid lines denote the measured output thruster force using Saturation Guard.

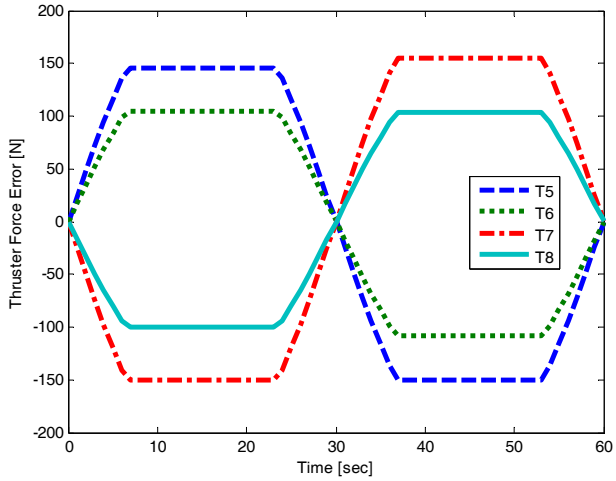

Fig. 13 Thruster force error with Saturation Guard.

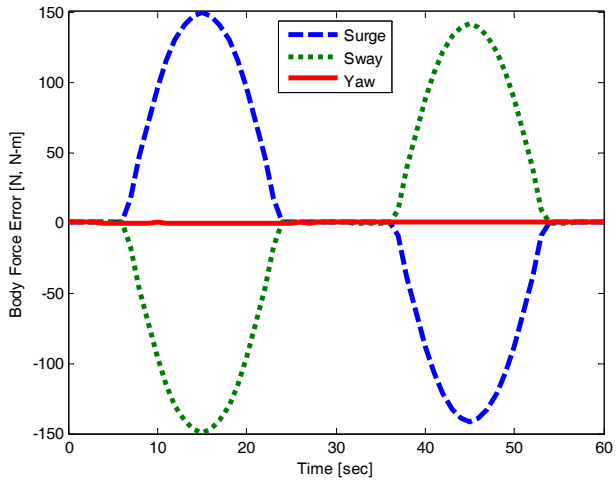

Fig. 14 Body force error with Saturation Guard.

ACKNOWLEDGMENTS

This research was sponsored in part by the NSF PYI Award (BES91-57896), NSF (BES97-01614, INT9603043), and ONR (N00014-97-1-0961, N00014-00-1-0629, N00014-02-1-0840).

REFERENCES

Bachmayer, R, Whitcomb, LL, and Grosenbaugh, MA (2000), "An accurate four-quadrant nonlinear dynamical model for marine thrusters: theory and experimental validation", *IEEE Journal of Oceanic Engineering*, Vol 25, No 1, pp 146 – 159.

Fossen, TI, and Blanke, M (2000), "Nonlinear output feedback control of underwater vehicle propellers using feedback from estimated axial flow velocity", *IEEE Journal of Oceanic Engineering*, Vol 25, No 2, pp 241 – 255.

Fossen, T (1994), "Guidance and Control of Ocean Vehicles", John Wiley & Sons, Chichester.

Kim, J, Han, J, Chung, WK, Yuh, J, and Lee, PM (2005) "Accurate and practical thruster modeling for underwater vehicles", *Proceedings of the 2005 IEEE International Conference on Robotics and Automation*, pp 175 – 180.

Nakamura, Y (1990), "Advanced Robotics: Redundancy and Optimization", Addison-Wesley Longman Publishing Co., Inc., Boston.

Sarkar, N, Podder, TK, and Antonelli, G (2002), "Fault-accommodating thruster force allocation of an AUV considering thruster redundancy and saturation", *IEEE Transactions on Robotics and Automation*, Vol 18, No 2, pp 223 – 233.

Smallwood, DA, and Whitcomb, LL (2002), "The effect of model accuracy and thruster saturation on tracking performance of model based controllers for underwater robotic vehicles: experimental results", *Proceedings of the 2002 IEEE International Conference on Robotics & Automation*, Vol 2, pp 1081 – 1087.

Smallwood, DA, and Whitcomb, LL (2004), "Model-based dynamic positioning of underwater robotic vehicles: theory and experiment", *IEEE Journal of Oceanic Engineering*, Vol 29, No 1, pp 169 – 186.

Soylu, S, Buckham, BJ, and Podhorodeski, RP (2007), "Robust control of underwater vehicles with fault-tolerant infinity-norm thruster force allocation", *Proceedings of MTS/IEEE Oceans 2007*, Vancouver, BC, Canada.

Yuh, J, and Choi, SK (1999), "Semi-Autonomous Underwater Vehicle for Intervention Missions (SAUVIM)", *Sea Technology*.